Breakpoint lead-lag analysis of the last deglacial climate change and atmospheric CO_2 concentration on global and hemispheric scales

Zhi Liu[a], Shaopeng Huang[a,b,*], Zhangdong Jin[c,a]

[a] School of Human Settlements and Civil Engineering, Xi'an Jiaotong University, Xi'an 710049, China
[b] Department of Earth and Environmental Sciences, University of Michigan, Ann Arbor, MI 48109-1063, USA
[c] State Key Laboratory of Loess and Quaternary Geology, Institute of Earth Environment, Chinese Academy of Sciences, Xi'an 710075, China

ABSTRACT

Antarctic ice core records show that climate change and atmospheric CO_2 concentration (aCO_2) are closely related over the past 800 thousand years. However, the interpretation of their sequential, and hence the causal relationship has long been controversial. In this study, we revisit this long-standing scientific issue based on 88 well-dated high-resolution climate proxy records derived from ice cores, marine deposits, and stalagmites. We composite global and hemispheric stacks of the last deglacial climate index (DCI) using a normalization scheme instead of a more conventional area-weighting and mixing scheme to enable a better detection of temporal variations. Rampfit and Breakfit techniques are employed to detect the trend transitions in each composited DCI series and in the recently constructed centennial-scale aCO_2 over the period from 22 to 9 thousand years before present. We detect a clear lead of DCI change over aCO_2 variation on both global and hemispheric scales at the early stage of the deglaciation, suggesting that the variation of aCO_2 is an internal feedback in Earth's climate system rather than an initial trigger of the last deglacial warming. During the periods of the Bølling-Allerød and the Younger Dryas, the climate system appeared to have been constrained by a fast coupling mechanism between climate change and aCO_2 with no obvious asynchrony. The northern and southern hemispheric DCI stacks exhibit a seesawing pattern that can be linked to the influences of Atlantic meridional overturning circulation (AMOC) strength, revealing an important role of AMOC in regulating the global climate in the course of the last deglaciation.

1. Introduction

Multiple glacial − interglacial cycles are the major characteristics of the Quaternary climate evolution. During the period from about 20 to 10 kabp (thousand years before present, where the present is A.D. 1950), the global climate emerged from the last glaciation; the global mean temperature went up by about 4–7 K (Guilderson et al., 1994; Dahl-Jensen et al., 1998; Farrera et al., 1999; Stenni et al., 2001; Ballantyne et al., 2005; Huang et al., 2008), the large northern hemispheric ice sheets retreated (Dyke, 2004), the global sea level rose over 120 m (Fleming et al., 1998; Clark et al., 2004; Peltier and Fairbanks, 2006; Lambeck et al., 2014), and the atmospheric carbon dioxide concentration (aCO_2) increased by about 80 ppmv (parts per million by volume) (Neftel et al., 1988; Fischer et al., 1999; Monnin et al., 2001; Ahn et al., 2004; Marcott et al., 2014). These changes, to some degree, are similar to what the human beings are facing at the present-day. Therefore the studies with respect to the process of the last deglaciation are relevant to the understanding of the modern climate change.

Antarctic ice core studies (Neftel et al., 1988; Fischer et al., 1999; Monnin et al., 2001; Ahn et al., 2004; Marcott et al., 2014) have provided clear evidences for a close relationship between surface air temperature (SAT) and aCO_2 variations during the last deglaciation. However, the questions such as which one changed first, and whether aCO_2 was a driver of this climate transformation or it was just a feedback that had enhanced the warming, have long been subjects of debate (Wolff, 2012; Brook, 2013). Existing ice core records of Byrd (Neftel et al., 1988), Taylor Dome (Fischer et al., 1999), Dome Concordia (Monnin et al., 2001), and Siple Dome (Ahn et al., 2004) show that the rise of aCO_2 lagged the rise of SAT, but the timescales of ice core records are complicated by the uncertainty of the gas-ice age difference (Δage) that caused by the hysteresis of the air bubble's formation relative to the surrounding ice. In the recent years, several advanced approaches have been developed to improve the determination of Δage. For example, using $\delta^{15}N$ data as a firn column depth indicator, Parrenin et al. (2012, 2013) revised the timescale of aCO_2 derived from the Dome Concordia ice core, and showed that the variations of aCO_2 and

---

Z. Liu et al. Quaternary International 490 (2018) 50–59

SAT were almost synchronous throughout the last deglaciation within an uncertainty less than 200 years. Similarly, the recently published centennial-scale aCO_2 record derived from the West Antarctic Ice Sheet Divide ice core (WDC) (Marcott et al., 2014) exhibits a nearly synchronous variation with SAT.

Another obstacle in our understanding of the sequential relationship between SAT and aCO_2 is the global/regional representativeness of the paleoclimatic records. Although the aCO_2 records derived from ice cores are viewed as global average because of air diffusion, the reconstructions of SAT based on the isotope ratios (e.g., $\delta^{18}O$ and δD) of individual ice cores reflect only local information that is generally mixed with non-climatic signals. In order to overcome these drawbacks, there have been great efforts aiming at a robust reconstruction of Antarctic SAT in the past few years. For instance, based on five coastal ice core proxy records, Pedro et al. (2011) composited an Antarctic SAT stack using the fast-changing global methane gas concentrations as the time markers. Through quantitative analysis of the time-lag between the composited SAT stack and two existing aCO_2 records, Pedro et al. (2012) concluded that the aCO_2 fell behind the Antarctic SAT by less than 400 years and could not exclude the possibility of a slight lead. On larger spatial scales, Shakun et al. (2012) synthesized global and hemispheric temperature stacks from 80 proxy reconstructions using a linear interpolation and area-weighting method to show that the global warming during the last deglaciation was preceded by the increase of aCO_2.

Although ice core record is a well-known indicator of paleoclimate change, information of climate change in the past are also preserved well in other media. In addition to 13 polar ice core records, we include in our database 58 marine sedimentary records of sea surface temperature and 17 stalagmite isotope records of precipitation information in this study to allow for a better global/hemispheric representativeness. We totally collect and collate 88 well-dated high-resolution proxy records over the last deglaciation as the underlying paleoclimatic database of this study. Using a straightforward scheme of normalization and moving average, we reconstruct global and hemispheric stacks of the last deglacial climate index (DCI) as a composited indicator of climate change for the period from 22 to 9 kabp. To determine the sequential relationships between the reconstructed stacks and aCO_2, we employ the techniques of Rampfit (Mudelsee, 2000) and Breakfit (Mudelsee, 2009) to detect the breakpoints in each composited DCI series and in the centennial-scale WDC aCO_2 (Marcott et al., 2014) for intercomparison. Finally, we discuss the driving mechanism of the last deglacial climate change.

2. Data and methods

2.1. The paleoclimatic database

88 well-dated high-resolution paleoclimatic records derived from ice cores, marine deposits, and stalagmites are collected and collated as the underlying database of this study. Spatially, the sites of these records cover broadly the globe (Fig. 1). Temporally, the average density over the period from 22 to 9 kabp is 136 measurements per hundred years with a total of 17,699 data points. The data density over the interval from 16 to 9 kabp is even higher. The data volumes are 11,655 for the Northern Hemisphere, and 6,044 for the Southern Hemisphere, respectively (Fig. 2A). General characteristics of these 88 records are given in the companion data article (Liu et al., 2018).

2.1.1. Ice core $\delta^{18}O$ and δD records

Both stable oxygen isotope ratio ($\delta^{18}O$) and stable hydrogen isotope ratio (δD) in ice cores can be analyzed to reflect glacial surface temperatures. The chronologies of ice core records depend mainly on the methods of layer-counting and glaciological models, as well as calibrations by other time markers such as methane, volcanic ash, and Beryllium-10. Our database includes 4 Greenlandic ($\delta^{18}O$) and 9

Antarctic (2 δD and 7 $\delta^{18}O$) ice core records. These records involve three representative timescales that focus on different correction methods and time markers. Therein, the chronologies of the 4 Greenlandic records, as well as the Antarctic records of Law Dome and Simple Dome, are based on the GICC05 timescale (Svensson et al., 2008), the Antarctic TALDICE, EDML, EDC, and Dome Fuji records are based on the AICC2012 timescale (Veres et al., 2013), and the Antarctic Taylor Dome, Vostok, and Byrd records are based on the Lemieux-Dudon timescale (Lemieux-Dudon et al., 2010). The average density of the ice core data is 44 measurements per hundred years with a total of 5,715 data points. The data volumes are smaller in the Northern Hemisphere than in the Southern Hemisphere (Fig. 2B).

2.1.2. Alkenone $U_{37}^{K'}$ and foraminifera Mg/Ca records

Alkenone ketone unsaturation index $U_{37}^{K'}$ and foraminifera Mg/Ca ratio of marine deposits are the indicators of sea surface temperatures. Reservoir effect is an important factor that must be taken into account in the radiocarbon dating of marine paleoclimatic records (Buck and Blackwell, 2004; Nakamura et al., 2016; Wang et al., 2017). With respect to the reservoir effect of ^{14}C dating, Shakun et al. (2012) made careful corrections of the radiocarbon-based timescales of 32 $U_{37}^{K'}$ and 26 Mg/Ca records based on the IntCal04 standard (Reimer et al., 2004) and Monte Carlo simulations. In our database, we include these 58 corrected records as the representations of marine region. Therein, 4,351 data points in total from 22 to 9 kabp are included, showing a relatively homogeneous distribution with the average density of 33 measurements per hundred years (Fig. 2C–E).

2.1.3. Stalagmite $\delta^{18}O$ records

The $\delta^{18}O$ records of stalagmites mainly reflect the information of precipitation or the intensity of monsoon. The patterns of the stalagmite-based reconstructions of precipitation and monsoon intensity have been showed to be analogous to the climate changes during the last deglaciation (e.g., Wang et al., 2001; Wang et al., 2007; Cheng et al., 2009; Cheng et al., 2013). Moreover, the accurate U-series-dating in stalagmites can provide an independent chronological constraint for the integration of the diverse paleoclimate records. In our database, all the chronologies of the 17 participant stalagmite records were derived from precise ^{230}Th absolute-dating. In comparison to other archives, the data density of stalagmite records with 7,632 data points exhibits a biggish fluctuation from 22 to 9 kabp and is denser in the Northern Hemisphere than in the Southern Hemisphere (Fig. 2F).

2.2. The WDC aCO_2 record

The WDC site is located in the western Antarctic (79.467° S, 112.085° W) with a high average snow accumulation rate of 22 cm/yr at the present-day. An accurate timescale since 30 kabp was established using the chronological method of annual layer counting. The Δage between the ice and the trapped gas was estimated to be 205 ± 10 years at the present and 525 ± 100 years at the last glacial maximum (Marcott et al., 2014). The high snow accumulation rate and precise chronological constraints enable a better-dated gas chronology and the reconstruction of aCO_2 at sub-centennial resolution.

2.3. Methods

2.3.1. Data synthesis

Most of the existing studies on global, hemispheric, and regional scales have been based on interpolated and area-weighted assembles of climatic time series. However, such a conventional interpolation and area-weighting method is not necessarily the best choice for integration of scattered paleoclimate records derived from diverse climate proxies and different geographical settings. For example, although they are all located in the Arctic region, five paleoclimatic records used in the study of Shakun et al. (2012) that reconstructed from ice core $\delta^{18}O$,
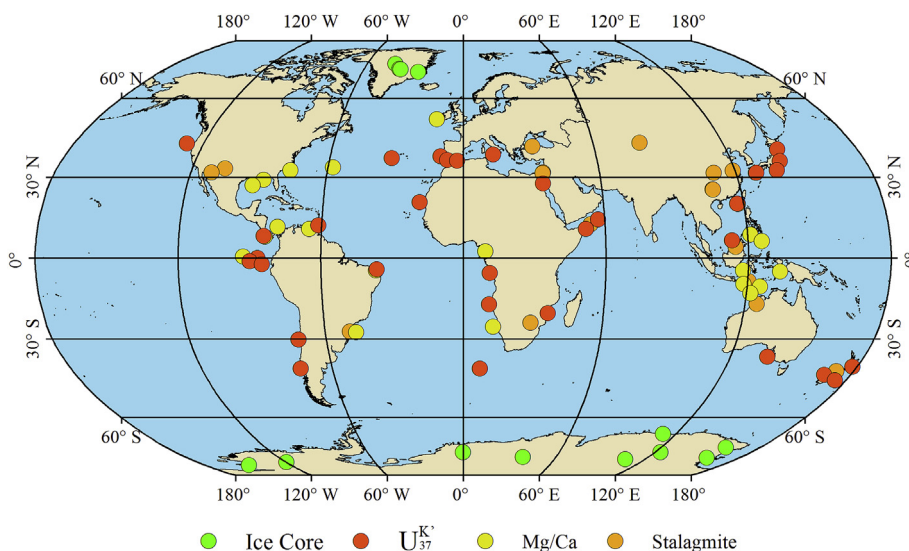
Fig. 1. Location map of the selected 88 paleoclimatic records of this study.

chironomid, and pollen respectively are very much different in their time resolution and inferred temperature range over the last deglacial period (Table 1). Individual reconstructions comprise measurements as many as 650 in the Greenlandic ice core record and as few as 38 in the Alaskan Burial Lake record during the interval from 22 to 9 kabp. The range between the maximum and minimum temperatures of a reconstruction varies from 4.1 to 32.5 K, whereas the early Holocene (11.5–9 kabp) mean temperature varies from −34.0 to 9.9 °C.
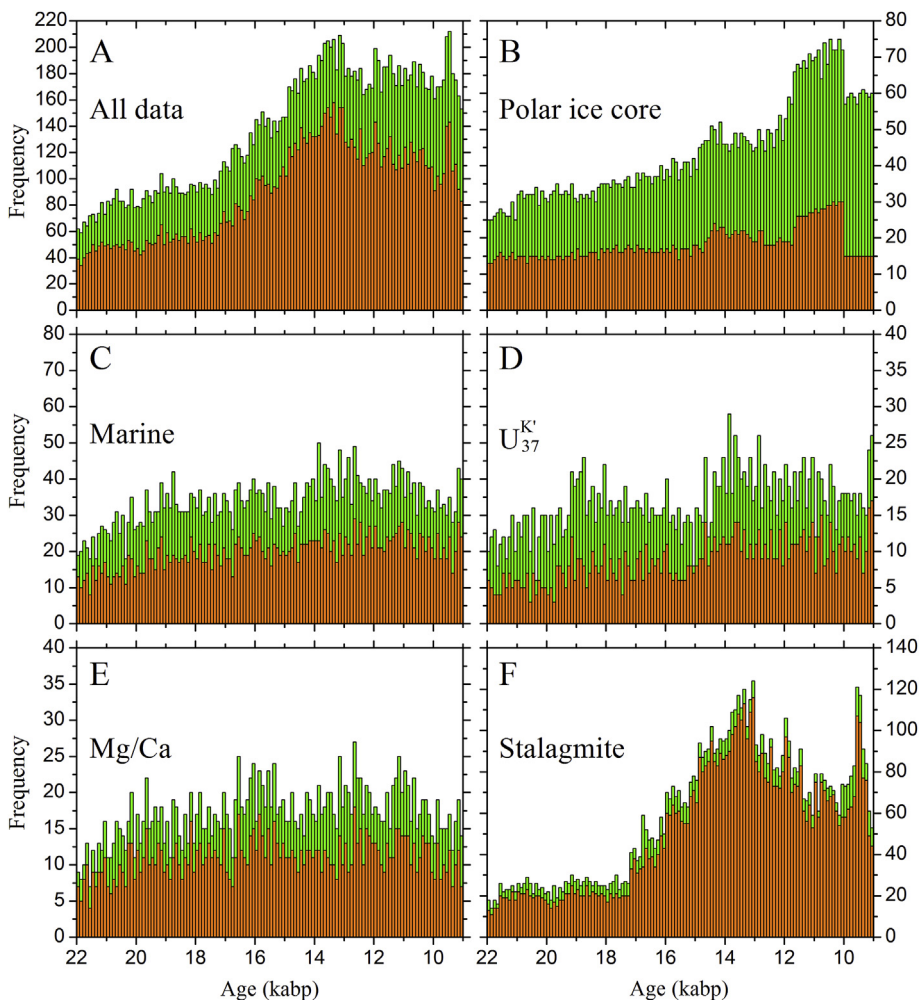

Fig. 2. Data densities of the participant paleoclimatic records in 100-year interval. Northern hemispheric data are showed in bronze and southern hemispheric data in green. (For interpretation of the references to color in this figure legend, the reader is referred to the Web version of this article.)

Table 1
Statistical characteristics of five proxy temperature reconstructions from 22 to 9 kabp in the Arctic region (Shakun et al., 2012)

Location	Proxy	Latitude	Longitude	Size	Min. (°C)	Max. (°C)	Range (K)	11.5–9 kabp mean (°C)
NGRIP, Greenland	$\delta^{18}O$	75.1	−42.3	650	−61.8	−29.3	32.5	−34.0
GRIP, Greenland	$\delta^{18}O$	72.6	−37.6	650	−54.9	−27.0	27.9	−33.2
Burial Lake, Alaska	Chironomid	68.4	−159.2	38	5.8	11.0	5.2	9.9
Eastern Beringia (A)	Pollen	67.5	−165.0	131	−4.6	−0.5	4.1	−1.3
Eastern Beringia (B)	Pollen	67.5	−137.5	131	−11.3	−0.1	11.2	−1.4
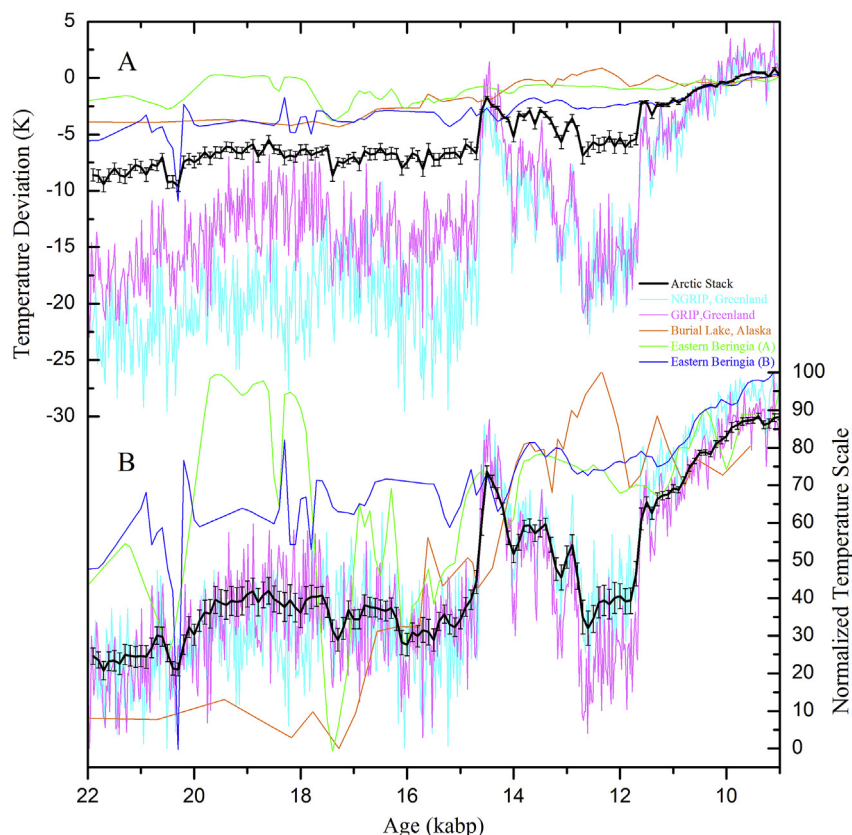
Fig. 3. Comparison between the stacks of five Arctic proxy temperature records with the linear interpolation and area-weighting scheme (A) and the normalization scheme (B). The interpolation interval is 100 years, and the area-weighting grid is 5° × 5° geographical coordinates. Error bars indicate 1σ errors.

Moreover, the commonly used area-weighting or cosine latitude weighting scheme would give a greater weight to the more uncertain pollen and chironomid records because of their lower latitudes than the higher latitude ice core records. Obviously, application of the conventional interpolation and area-weighting scheme to such diverse reconstructions for a regional representation is irrational. Nevertheless, each of the reconstruction comprises valuable information regarding the climate change. A more reasonable approach to synthesize such paleoclimatic records would be to normalize each of them before integration. Fig. 3 shows as an example for comparing the integrations of Arctic temperature based on these five proxy records to illustrate the difference between the conventional interpolation and area-weighting scheme and a straightforward data normalization scheme. It is obvious that the area-weighted stack of the linearly interpolated face values of these proxy records can hardly be representative of the last deglacial climate in this region (Fig. 3A). In contrast, the data normalization scheme allows for a better multiproxy integration and regional representation (Fig. 3B).

Polar ice core records provide abundant information for paleoclimatology and the natural evidence supporting the close relationship between climate change and aCO₂ (e.g., Neftel et al., 1988; Fischer et al., 1999; Petit et al., 1999; Monnin et al., 2001; Ahn et al., 2004;

Lüthi et al., 2008; Marcott et al., 2014). Additionally, the chronology of ice cores, determined by a variety of methods, is an important element in calibrating dates of other paleoclimatic records. Despite that the marine alkenone $U^{K'}_{37}$ and foraminifera Mg/Ca records reconstructed in many studies share agreements in patterns and timings with the polar ice core records (e.g., Lea et al., 2003; Benway et al., 2006; Peck et al., 2008; Barker et al., 2009), their resolution is relatively lower. In regard to the stalagmite proxies, existing studies have shown that the patterns of stalagmite $\delta^{18}O$ records are comparable to the polar ice core records (e.g., Wang et al., 2001; Wang et al., 2004; Cruz et al., 2005; Cheng et al., 2009; Asmerom et al., 2010; Ayliffe et al., 2013; Cheng et al., 2016). Especially, the absolute ²³⁰Th dating of stalagmite proxies could provide an independent constraint for the temporal variations of the integration. However, the amplitudes of the reconstructions from different paleoclimatic proxies are divergent. The systematic discrepancies in temporal resolutions and amplitude ranges of the different proxy records in our database are significant and cannot be ignored. The comparability of these different proxy records needs to be addressed before synthesis.

Given the heterogeneous and sporadic nature of the underlying database, and given that the major interest of this study is on the timing of the changes in climate trend rather than the absolute magnitude of
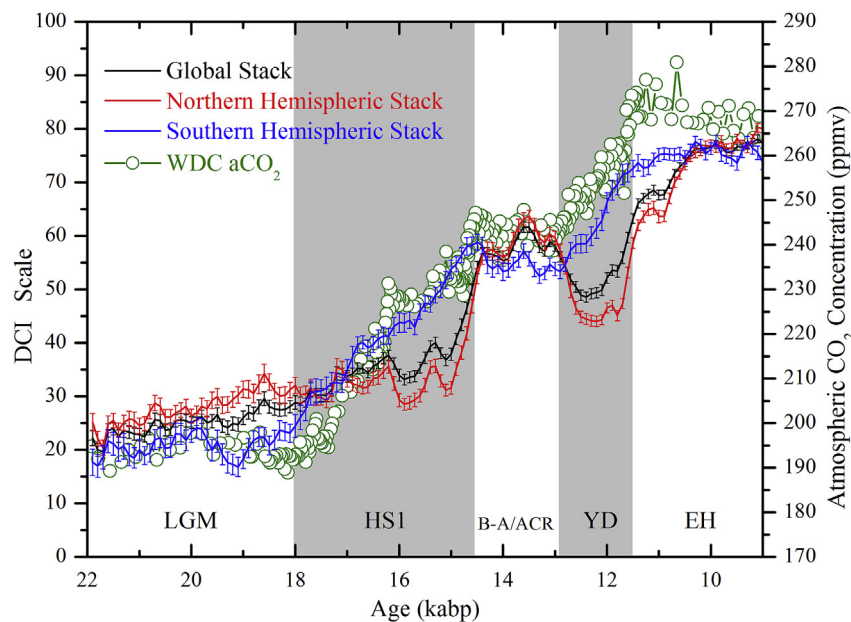
Fig. 4. Global and hemispheric DCI stacks overlaid on the centennial-scale WDC aCO₂ (Marcott et al., 2014). The error bars indicate 1σ errors. LGM: Last Glacial Maximum; HS1: Heinrich Stadial 1; B–A: Bølling-Allerød; ACR: Antarctic Cold Reversal; YD: Younger Dryas; EH: Early Holocene.

climate variation, we chose the normalization scheme in this study to reconstruct the global and hemispheric DCI stacks. First, we normalized all the 88 participant proxy records separately to a 0–100 scale based on the maximum-minimum range (Supplementary Materials Part 1). Then, the normalized data were averaged using a 200-year moving window with a 100-year overlap to reconstruct the 100-year resolution stacks of the global and hemispheric ensembles. This straightforward scheme synthesized time series comprising paleoclimate information of surface air temperature changes from the ice core records, sea surface temperature variations from the marine sediments, and precipitation information from the stalagmite data. The resultant stacks are composite paleoclimate indexes over the last deglaciation period.

2.3.2. Breakpoint detections

Using a continuous linear piecewise model to fit the paleoclimate record is a widely used approach in breakpoint analysis of paleoclimate time series (e.g., Monnin et al., 2001; Parrenin et al., 2013). We employed the techniques of Rampfit and Breakfit both developed by Mudelsee (2000, 2009) to detect the breakpoints in each reconstructed DCI series, as well as in the WDC aCO₂ series (Marcott et al., 2014) which was interpolated linearly to a 100-year resolution from 22 to 9 kabp. The Rampfit and Breakfit are least-squares regression techniques based on Ramp function and Break function, respectively, for quantifying the trend changes in a time series. In general, the Rampfit technique is more suitable for slope-shape series, whereas the Breakfit technique is more suitable for V-shape series. We employed both methods for cross verification and comparison. According to the patterns of the reconstructed stacks, we selected five time windows of 22–16.5 kabp, 16.5–14.5 kabp, 15–13 kabp, 14.5–12.5 kabp for Breakfit technique, and 12.5–9 kabp for Rampfit technique to detect the timings of six breakpoints in the global and northern hemispheric DCI stacks, two time windows of 22–13 kabp and 14–9 kabp for Rampfit technique to detect the timings of four breakpoints in the southern hemispheric DCI stack, and three time windows of 22–15.5 kabp, 16–13 kabp, and 14–9 kabp for Rampfit technique to detect the timings of six breakpoints in the WDC aCO₂ series. In our analysis, 500 bootstrap simulations were repeated to generate the standard deviations.

3. Results

3.1. 100-year resolution global and hemispheric DCI stacks

Fig. 4 shows the stacks of the global and hemispheric DCI with 100-year resolution from 22 to 9 kabp. The major feature of the global stack is an increase from a mean value of 22 between 22 and 19 kabp to a mean value of 77 between 10 and 9 kabp in the DCI scale. The rise of the 55 DCI units occurred mainly in two steps; the first step happened during ~15 to 14.5 kabp that corresponding to the transformation from the Heinrich Stadial 1 (HS1) to the Bølling-Allerød (B-A) warm period with an increase of approximate 20 DCI units, whereas the second-step rising of about 30 DCI units took place during ~12.6 to 10.3 kabp corresponding to the ending of the Younger Dryas (YD). In addition, a gradual increase occurred over the Last Glacial Maximum (LGM) and the HS1 with more than 10 DCI units.

The northern hemispheric DCI likewise shows a two-step increase as seen in the global DCI. However, a significant difference is that, after the transformation from LGM to HS1 the increase rate of DCI slowed down in the northern hemispheric stack, where it was accelerated in the global stack. In the Southern Hemisphere, similar to the patterns of Antarctic ice core records (Neftel et al., 1988; Fischer et al., 1999; Monnin et al., 2001; Ahn et al., 2004; Marcott et al., 2014), the DCI stack shows a parallel variation with the WDC aCO₂ (Marcott et al., 2014), both experienced two rapid increasing phases, HS1 and YD, separated by the Antarctic Cold Reversal (ACR) event.

The similarity in the patterns between the southern hemispheric DCI stack and the WDC aCO₂ supports the hypothesis that the Southern Ocean played an important role in the deglacial aCO₂ rising (Sigman et al., 2010). Meanwhile, the comparison of changes between the northern and southern hemispheric DCI stacks shows an obvious seesawing characteristic, demonstrating the effects of Atlantic meridional overturning circulation (AMOC) on the interhemispheric redistribution of heat (Broecker, 1998; Stocker and Johnsen, 2003; Denton et al., 2010).

3.2. Breakpoint detections of trend transitions

Fig. 5 shows the detection of the breakpoints in the reconstructed DCI stacks, as well as in the WDC aCO₂ series. The results are
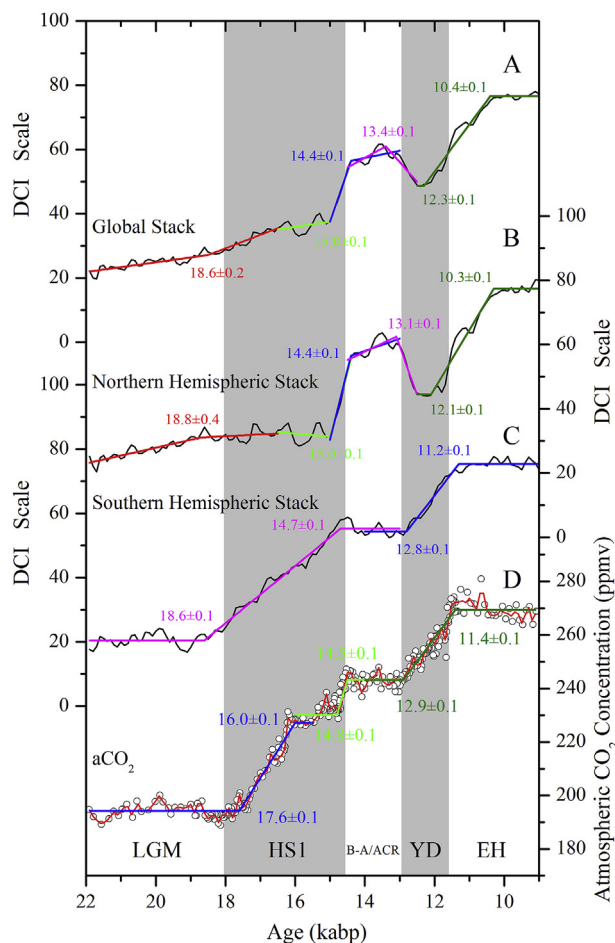
Fig. 5. Detection of breakpoints in the global/hemispheric DCI stacks and aCO₂ (Marcott et al., 2014). The polylines in color are the least-square regressions based on the techniques of Rampfit/Breakfit (Mudelsee, 2000, 2009). Errors of all the detected results are the standard deviations of 500 repeated bootstrap simulations. The gray hollow dots in panel (D) are the originally centennial-scale WDC aCO₂ data, and the overlaid red line is the linearly interpolated series of 100-year resolution. The codes of the climate events are the same as in Fig. 4. (For interpretation of the references to color in this figure legend, the reader is referred to the Web version of this article.)

summarized in Table 2. Five breakpoints at best are intercomparable among the global/hemispheric DCI stacks and aCO₂. Breakpoint 1 corresponds to the transformation from LGM to HS1 in the global and northern hemispheric DCI stacks, and the onset of the deglaciation in the southern hemispheric DCI stack and aCO₂. Breakpoint 2 marks the onset of the transformation from HS1 to B-A. Breakpoint 3 corresponds to the onset of B-A in the global and northern hemispheric DCI stacks, which can be correlated with the onset of ACR in the southern hemispheric DCI stack and aCO₂. Breakpoint 4 indicates the ending of B-A in the global and northern hemispheric DCI stacks, and the ending of ACR in the southern hemispheric DCI stack and aCO₂. Breakpoint 5 corresponds to the endpoint of the deglaciation.

The comparison of five breakpoints between the global DCI stack

and aCO₂ (Fig. 5A, D; Table 2) comprises three different sequential relationships. (i) The significant rising of aCO₂ started at 17.6 ± 0.1 kabp lagged behind the onset of global climate change that occurred earlier than 18.6 ± 0.2 kabp. (ii) During the B-A warm period, aCO₂ and the global DCI had an almost synchronous variation most time with no more than 500-year difference. This is similar to the recent results of Pedro et al. (2012), Parrenin et al. (2013), Rosen et al. (2014), and Bereiter et al. (2018). (iii) The aCO₂ hiatus post YD began at about 11.4 ± 0.1 kabp, leading the termination of the YD around 10.4 ± 0.1 kabp by about 1000 years.

As mentioned above, the northern hemispheric DCI stack shows a similar pattern to the global DCI stack except for the changing trend after the transformation from LGM to HS1. Our analysis indicates that this transformation took place around 18.8 ± 0.4 kabp, leading the onset of aCO₂ rising by more than 1200 years (Fig. 5B, D; Table 2). In contrast to the northern hemispheric DCI stack, parallel variations between the southern hemispheric DCI stack and aCO₂ make it easier to compare the order of the breakpoints (e.g., Mudelsee, 2001; Ahn et al., 2004; Siegenthaler et al., 2005; Pedro et al., 2012). Four breakpoints are comparable between the southern hemispheric DCI stack and aCO₂ that suggest a more than 1000-year lead of DCI change over aCO₂ variation at the early stage of the deglaciation, a synchronous variation within 200-year time difference during the ACR period, and a less than 200-year lag at the ending of the deglaciation (Fig. 5C–D; Table 2). In addition to the seesawing characteristics between the Northern and Southern Hemispheres, four pairs of comparable breakpoints between the two hemispheric DCI stacks indicate nearly contemporaneous transformations of climatic trends in the interval from LGM to early Holocene by less than 300-year difference except the ending point of the deglaciation (Fig. 5B–C; Table 2), reflecting a close interhemispheric correlation.

Overall, the results of breakpoint analyses on global and hemispheric scales show a clear DCI lead over aCO₂ at the early stage of the deglacial warming, suggesting that aCO₂ is an internal feedback in Earth's climate system rather than an initial trigger. The nearly synchronous change between the global/hemispheric DCI stacks and aCO₂ during the B-A warm period (i.e., the ACR period in the Southern Hemisphere) suggests a fast coupling between the variations of climate and aCO₂.

4. Discussion

4.1. Comparison between the normalization and area-weighting schemes

Given the diverse temporal resolutions and sparse nature of the existing paleoclimate records as well as the complexity of the climate system, identifying the sequential and causal relationship between climate change and aCO₂ variation remains a challenging task and requires continued efforts using improved methods. One important difference of this study from previous studies lies in the application of normalization as opposed to area-weighting approach to synthesize diverse multiple proxy records for global and hemispheric representations. With the normalization approach, we show a climate–aCO₂ variation sequential relationship somewhat different from what have been reported by some existing studies. For example, using a linearly interpolated and area-weighted method, Shakun et al. (2012) synthesized

Table 2
Detected breakpoints in the global/hemispheric DCI stacks and WDC aCO₂ (Unit: kabp).

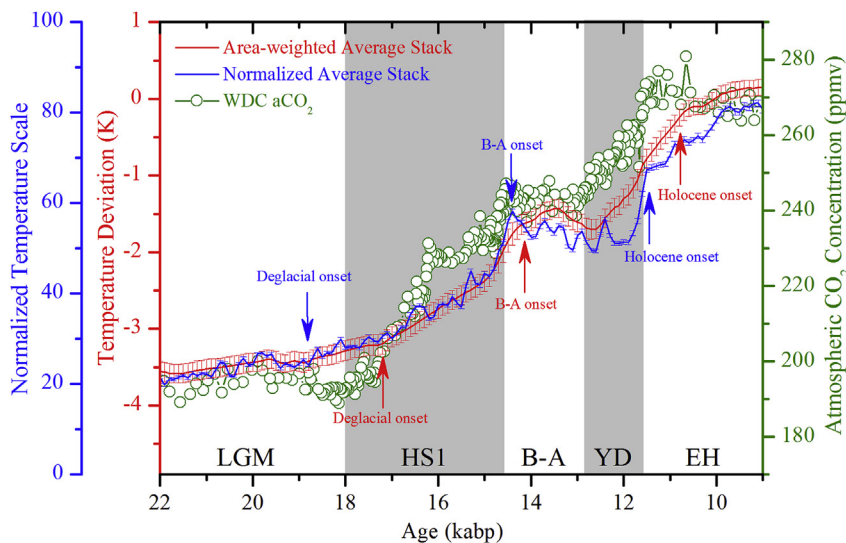|	Breakpoint 1	Breakpoint 2	Breakpoint 3	Breakpoint 4	Breakpoint 5
Global DCI	18.6 ± 0.2	15.0 ± 0.1	14.4 ± 0.1	13.4 ± 0.1	10.4 ± 0.1
Northern Hemisphere DCI	18.8 ± 0.4	15.0 ± 0.1	14.4 ± 0.1	13.1 ± 0.1	10.3 ± 0.1
Southern Hemisphere DCI	18.6 ± 0.1		14.7 ± 0.1	12.8 ± 0.1	11.2 ± 0.1
WDC aCO₂	17.6 ± 0.1	14.8 ± 0.1	14.5 ± 0.1	12.9 ± 0.1	11.4 ± 0.1

Fig. 6. Normalized and area-weighted global climate stacks based on Shakun et al. (2012) 80 proxy records during the last deglaciation in comparison to the centennial-scale WDC aCO$_2$ (Marcott et al., 2014). The error bars indicate 1σ errors. The arrows highlight some change/event onsets interpreted from normalization method (blue) and area-weighting method (red), respectively. The codes of the climate events are the same as in Fig. 4. (For interpretation of the references to color in this figure legend, the reader is referred to the Web version of this article.)

the global and hemispheric stacks of the last deglacial temperature from 80 proxy records to show that the global warming was preceded by the increase of aCO$_2$. Their study exhibited a lead of 460 ± 340 years of aCO$_2$ over the global temperature stack, a lead of 720 ± 330 years of aCO$_2$ over the northern hemispheric temperature stack, and a lag of 620 ± 660 years of aCO$_2$ over the southern hemispheric temperature stack (Pedro et al., 2012). However, we did not see in our reconstructed DCI stacks the major features upon which Shakun et al. (2012) developed their discussion and conclusion, despite that we included quite a few records from Shakun et al. (2012) database in our study.

For a more direct comparison, we recalculated the global and hemispheric stacks using the normalization scheme on the basis of the original 80 proxy records of Shakun et al. (2012). Our stacks bear some features that are significantly different from that of the area-weighted stacks of Shakun et al. (2012), leading to different interpretations of the timing of climate events (Supplementary Materials Part 3). For example, Shakun et al. (2012) regarded 17.2 ± 0.03 kabp as the onset of the deglacial warming substantially lagging the onset of aCO$_2$ rising; whereas 17.2 ± 0.03 kabp is not a breakpoint in the global stack using normalization scheme. Additionally, the onsets of the Bølling-Allerød and the Holocene can be timed earlier in the normalized stack than in the area-weighted stack (Fig. 6).

The data synthesis method of Shakun et al. (2012) included several steps: linear interpolation of the time series to a 100-year resolution, projection of the time series onto a 5° × 5° grid, and combination of the data for area-weighted stacks. However, this method may not fit the underlying proxy database. First, although the proxy measurements of each participant reconstruction may be of sufficient qualities and internally consistent, there are obviously systematic discrepancies among the participant reconstructions due to different proxies and methodologies used. The discrepancies can impose serious biases to the global and hemispheric ensembles if unaccounted for. Second, overstretching a low-density reconstruction to a 100-year resolution would inadvertently introduce artifacts into the ensembles, especially for the marine sedimentary records with relatively lower data density. Moreover, the 5° × 5° grid weighting scheme attaches the weight of a proxy reconstruction to its geographical coordinates, which would promote the lower latitude records over the more robust ice core records.

4.2. Driving mechanism of the last deglacial climate change

Our analysis shows that during the initial stage of the last deglaciation, the rise in aCO$_2$ was preceded by the rise in DCI, reconfirming the finding of several earlier studies (e.g., Fischer et al., 1999; Monnin et al., 2001; Fudge et al., 2013) that aCO$_2$ elevation is not the trigger of

the deglacial warming. This is consistent with the Milankovitch theory that postulated the variation of summer insolation at northern high latitude as the driving force of the glacial-interglacial cycles of late Quaternary (Milanković, 1941; Hays et al., 1976). Summer solar insolation began to increase from its minimum level about 24 kabp in high-latitude Northern Hemisphere (Laskar et al., 2004) (Fig. 7A). The increasing insolation caused the Northern Hemisphere warming, as evidenced in the moderate warming in the very early stage of deglaciation from 22.0 to 18.8 kabp shown in Fig. 7D. However, the initial Northern Hemisphere warming did not appear to continue into HS1. The absence of an apparent 18.8–15.0 kabp Northern Hemisphere warming might have been a side effect of the early deglacial melting of the northern ice sheets. Coupled atmosphere-ocean general circulation model simulation (Liu et al., 2009; Marcott et al., 2011) suggested that the insolation induced warming over this period could have been hidden in the subsurface ocean waters. Surface freshening in the early stage of the deglaciation could suppress convective heat exchange, resulting in cooling the surface while warming the subsurface (Liu et al., 2009). The deglacial warming subsequently led to the generation of vast sea ice (Raymo et al., 1997; Denton et al., 2010) and the occurrence of ice rafting (Heinrich, 1988; Stern and Lisiecki, 2013) (Fig. 7B).

On the millennial scale, the injection of meltwater into the North Atlantic Ocean would reduce the strength of AMOC (Ganopolski and Rahmstorf, 2001; McManus et al., 2004) (Fig. 7C) through weakening the formation of deep water. This would decrease the heat transferred from the low latitude area. The effect of the bipolar seesaw (Broecker, 1998; Stocker and Johnsen, 2003; Denton et al., 2010) could then lead to the initial warming of the Southern Hemisphere (Ganopolski and Roche, 2009; He et al., 2013) (Fig. 7E) and a pause of the Northern Hemisphere warming (Fig. 7D). Meanwhile, the reduction of the AMOC strength, and the drift southward of icebergs and sea ices, could jointly push the Intertropical Convergence Zone and Southern Hemisphere Westerlies to move southward (Chiang and Bitz, 2005). These effects would enhance the ventilation between the Southern Ocean and atmosphere (Anderson et al., 2009; Fischer et al., 2010) (Fig. 7F), and finally lead to vast CO$_2$ stored in the deep ocean being released to atmosphere (Clark et al., 2002; Schmittner and Galbraith, 2008; Sigman et al., 2010; Skinner et al., 2010), causing the rising of aCO$_2$ (Fig. 7G). During the B-A warm period and YD cold period, the seesawing features between the climate of Northern Hemisphere and Southern Hemisphere is likely an indication of the predominance of AMOC in regulating the interhemispheric climate change through reducing/increasing northward ocean heat transport and accordingly promoting/lowering the heat accumulation in the south (Fig. 7C–E). The near-synchronous variations between the southern hemispheric DCI and aCO$_2$ are
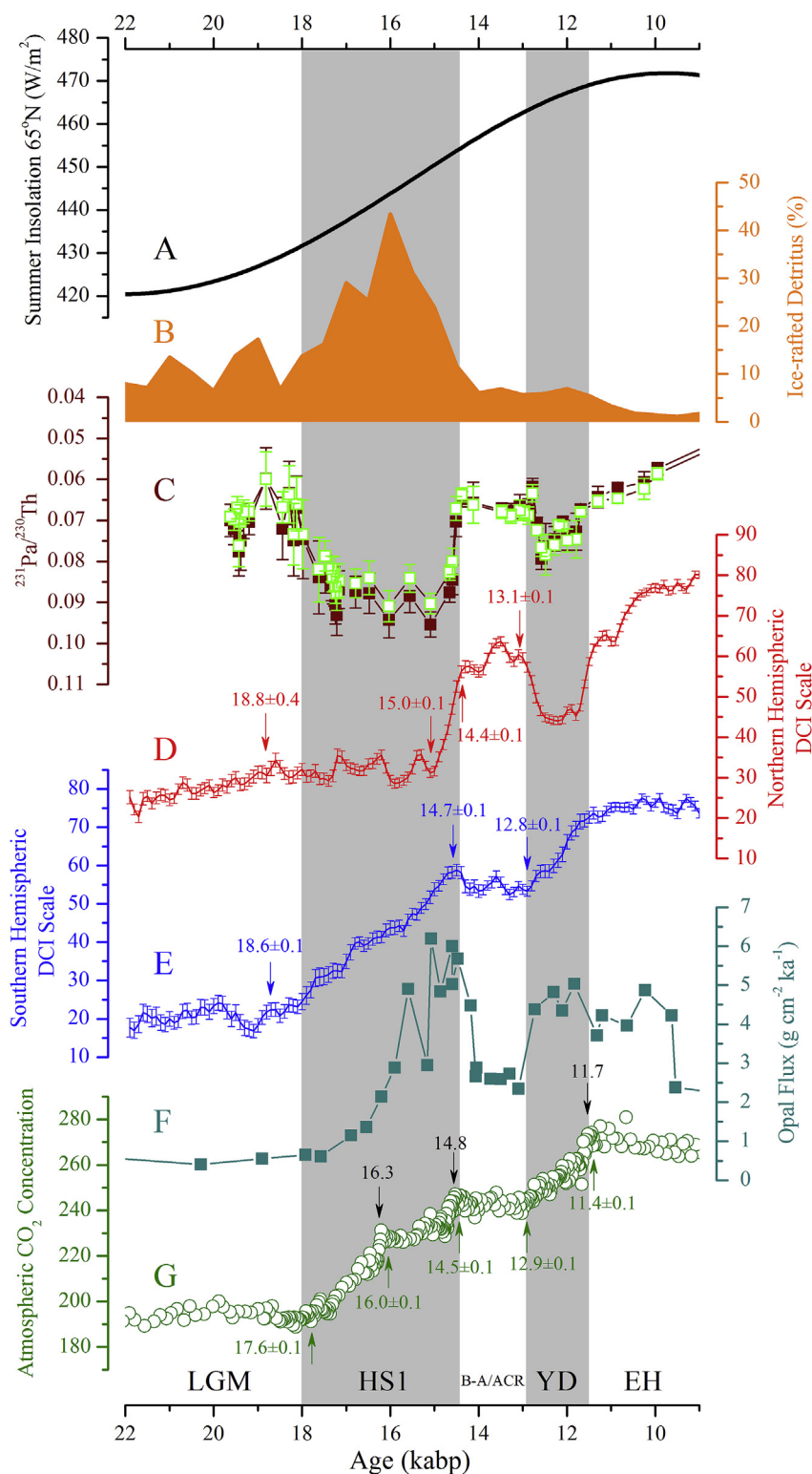
Fig. 7. Comparisons among multiple paleoenvironmental proxies over the deglaciation period from 22 to 9 kabp. (A) Summer insolation at 65° N (Laskar et al., 2004). (B) Ice-rafted detritus stack (Stern and Lisiecki, 2013). (C) The $^{231}Pa/^{230}Th$ ratios from the marine core OCE326-GGC5 as a proxy reflecting the strength of AMOC (McManus et al., 2004). (D) Northern hemispheric DCI stack. (E) Southern hemispheric DCI stack. (F) Opal flux from the marine core TN057-13PC4 located in the Southern Ocean, interpreted as a proxy for upwelling south of the Antarctic Polar Front (Anderson et al., 2009). (G) Centennial-scale WDC aCO$_2$ with black arrows to indicate the three abrupt rising (Marcott et al., 2014). The color arrows in the panels (D), (E), and (G) pointing some remarkable breakpoints detected in this study. The codes of the climate events are the same as in Fig. 4. (For interpretation of the references to color in this figure legend, the reader is referred to the Web version of this article.)

consistent with suggestions of a fast coupling between climate and aCO$_2$ changes (Pedro et al., 2012; Parrenin et al., 2013; Bereiter et al., 2018). The fast coupling is likely a consequence of an increased Southern Ocean overturning rate which concurrently enhanced the ocean-atmosphere heat and CO$_2$ exchanges (Anderson et al., 2009; Skinner et al., 2010).

On the centennial scale, Marcott et al. (2014) showed three rapid rising events of the WDC aCO$_2$ at 16.3 kabp, 14.8 kabp, and 11.7 kabp, respectively, and found all of them can be closely correlated to the

abrupt climate changes in the Northern Hemisphere. In the northern hemispheric DCI stack of this study, these correlations are also observable; three abrupt climate changes in the DIC scale at about 16.3 kabp, 14.4 kabp, and 11.2 kabp can be related to those rapid aCO$_2$ increases (Fig. 7D, G). These rapid changes of climate and aCO$_2$ correlate in time with the abrupt variations in the AMOC strength (McManus et al., 2004) and with the deposits of ice-rafted detritus in the North Atlantic (Stern and Lisiecki, 2013), suggesting that the AMOC had an important role in the abrupt rising of aCO$_2$ (Marcott et al.,

2014).

5. Conclusion

We use a normalization scheme to synthesize global and hemispheric stacks of composite climate index DCI from 88 well-dated high-resolution proxy records. Breakpoint analysis of the DCI stacks and the aCO_2 record from the West Antarctic Ice Sheet Divide ice core (Marcott et al., 2014) shows a varying lead-lag relationship over the period of the last deglaciation. The onset of DCI increase led the onset of aCO_2 rising on both global and hemispheric scales at the early stage of the last deglaciation, indicating that the variation of aCO_2 is an internal feedback in Earth's climate system rather than an initial trigger. The seesawing pattern between the northern and southern hemispheric DCI during the Bølling-Allerød warm period and the Younger Dryas cold period is likely a result of the predominance of AMOC in regulating the interhemispheric climate change. The near-synchronous variations of climate change and aCO_2 since the onset of the Bølling-Allerød can be attributed to the enhanced ventilation between the Southern Ocean and atmosphere.

Acknowledgments

Appendix A. Supplementary data

Supplementary data related to this article can be found at http://dx.doi.org/10.1016/j.quaint.2018.05.021.

References

Ahn, J., Wahlen, M., Deck, B.L., Brook, E.J., Mayewski, P.A., Taylor, K.C., White, J.W.C., 2004. A record of atmospheric CO_2 during the last 40,000 years from the Siple Dome, Antarctica ice core. J. Geophys. Res. Atmos. 109, 121–134.

Anderson, R.F., Ali, S., Bradtmiller, L.I., Nielsen, S.H.H., Fleisher, M.Q., Anderson, B.E., Burckle, L.H., 2009. Wind-driven upwelling in the Southern Ocean and the deglacial rise in atmospheric CO_2. Science 323, 1443–1448.

Asmerom, Y., Polyak, V.J., Burns, S.J., 2010. Variable winter moisture in the southwestern United States linked to rapid glacial climate shifts. Nat. Geosci. 3, 114–117.

Ayliffe, L.K., Gagan, M.K., Zhao, J.X., Drysdale, R.N., Hellstrom, J.C., Hantoro, W.S., Griffiths, M.L., Scott-Gagan, H., St Pierre, E., Cowley, J.A., Suwargadi, B.W., 2013. Rapid interhemispheric climate links via the Australasian monsoon during the last deglaciation. Nat. Commun. 4, 2908.

Ballantyne, A.P., Lavine, M., Crowley, T.J., Liu, J., Baker, P.B., 2005. Meta-analysis of tropical surface temperatures during the last glacial maximum. Geophys. Res. Lett. 32 L05712.

Barker, S., Diz, P., Vautravers, M.J., Pike, J., Knorr, G., Hall, I.R., Broecker, W.S., 2009. Interhemispheric Atlantic seesaw response during the last deglaciation. Nature 457, 1097–1102.

Benway, H.M., Mix, A.C., Haley, B.A., Klinkhammer, G.P., 2006. Eastern Pacific Warm Pool paleosalinity and climate variability: 0-30 kyr. Paleoceanography 21, PA3008.

Bereiter, B., Shackleton, S., Baggenstos, D., Kawamura, K., Severinghaus, J., 2018. Mean global ocean temperatures during the last glacial transition. Nature 553, 39–44.

Broecker, W.S., 1998. Paleocean circulation during the last deglaciation: a bipolar seesaw? Paleoceanography 13, 119–121.

Brook, E.J., 2013. Leads and lags at the end of the last ice age. Science 339, 1042–1043.

Buck, C.E., Blackwell, P.G., 2004. Formal statistical models for estimating radiocarbon calibration curves. Radiocarbon 46, 1093–1102.

Cheng, H., Edwards, R.L., Broecker, W.S., Denton, G.H., Kong, X.G., Wang, Y.J., Zhang, R., Wang, X.F., 2009. Ice age terminations. Science 326, 248–252.

Cheng, H., Edwards, R.L., Sinha, A., Spötl, C., Yi, L., Chen, S., Kelly, M., Kathayat, G., Wang, X., Li, X., Kong, X., Wang, Y., Ning, Y., Zhang, H., 2016. The Asian monsoon over the past 640,000 years and ice age terminations. Nature 534, 640–646.

Cheng, H., Sinha, A., Cruz, F.W., Wang, X., Edwards, R.L., d'Horta, F.M., Ribas, C.C., Vuille, M., Stott, L.D., Auler, A.S., 2013. Climate change patterns in Amazonia and biodiversity. Nat. Commun. 4, 1411.

Chiang, J.C.H., Bitz, C.M., 2005. Influence of high latitude ice cover on the marine Intertropical Convergence Zone. Clim. Dynam. 25, 477–496.

Clark, P.U., McCabe, A.M., Mix, A.C., Weaver, A.J., 2004. Rapid rise of sea level 19,000 years ago and its global implications. Science 304, 1141–1144.

Clark, P.U., Pisias, N.G., Stocker, T.F., Weaver, A.J., 2002. The role of the thermohaline circulation in abrupt climate change. Nature 415, 863–869.

Cruz, F.W., Burns, S.J., Karmann, I., Sharp, W.D., Vuille, M., Cardoso, A.O., Ferrari, J.A., Dias, P.L.S., Viana, O., 2005. Insolation-driven changes in atmospheric circulation over the past 116,000 years in subtropical Brazil. Nature 434, 63–66.

Dahl-Jensen, D., Mosegaard, K., Gundestrup, N., Clow, G.D., Johnsen, S.J., Hansen, A.W., Balling, N., 1998. Past temperatures directly from the Greenland ice sheet. Science 282, 268–271.

Denton, G.H., Anderson, R.F., Toggweiler, J.R., Edwards, R.L., Schaefer, J.M., Putnam, A.E., 2010. The last glacial termination. Science 328, 1652–1656.

Dyke, A.S., 2004. An outline of North American deglaciation with emphasis on central and northern Canada. Dev. Quat. Sci. 2, 373–424.

Farrera, I., Harrison, S.P., Prentice, I.C., Ramstein, G., Guiot, J., Bartlein, P.J., Bonnefille, R., Bush, M., Cramer, W., von Grafenstein, U., Holmgren, K., Hooghiemstra, H., Hope, G., Jolly, D., Lauritzen, S.-E., Ono, Y., Pinot, S., Stute, M., Yu, G., 1999. Tropical climates at the Last Glacial Maximum: a new synthesis of terrestrial palaeoclimate data. I. Vegetation, lake-levels and geochemistry. Clim. Dynam. 15, 823–856.

Fischer, H., Schmitt, J., Lüthi, D., Stocker, T.F., Tschumi, T., Parekh, P., Joos, F., Köhler, P., Völker, C., Gersonde, R., Barbante, C., Le Floch, M., Raynaud, D., Wolff, E., 2010. The role of Southern Ocean processes in orbital and millennial CO_2 variations–A synthesis. Quat. Sci. Rev. 29, 193–205.

Fischer, H., Wahlen, M., Smith, J., Mastroianni, D., Deck, B., 1999. Ice core records of atmospheric CO_2 around the last three glacial terminations. Science 283, 1712–1714.

Fleming, K., Johnston, P., Zwartz, D., Yokoyama, Y., Lambeck, K., Chappell, J., 1998. Refining the eustatic sea-level curve since the Last Glacial Maximum using far- and intermediate-field sites. Earth Planet Sci. Lett. 163, 327–342.

Fudge, T.J., Steig, E.J., Markle, B.R., Schoenemann, S.W., Ding, Q., Taylor, K.C., McConnell, J.R., Brook, E.J., Sowers, T., White, J.W.C., 2013. Onset of deglacial warming in West Antarctica driven by local orbital forcing. Nature 500, 440–444.

Ganopolski, A., Rahmstorf, S., 2001. Rapid changes of glacial climate simulated in a coupled climate model. Nature 409, 153–158.

Ganopolski, A., Roche, D.M., 2009. On the nature of lead-lag relationships during glacial-interglacial climate transitions. Quat. Sci. Rev. 28, 3361–3378.

Guilderson, T.P., Fairbanks, R.G., Rubenstone, J.L., 1994. Tropical temperature variations since 20,000 years ago: modulating interhemispheric climate change. Science 263, 663–665.

Hays, J.D., Imbrie, J., Shackleton, N.J., 1976. Variations in the Earth's orbit: pacemaker of the ice ages. Science 194, 1121–1132.

He, F., Shakun, J.D., Clark, P.U., Carlson, A.E., Liu, Z., Otto-Bliesner, B.L., Kutzbach, J.E., 2013. Northern Hemisphere forcing of Southern Hemisphere climate during the last deglaciation. Nature 494, 81–85.

Heinrich, H., 1988. Origin and consequences of cyclic ice rafting in the Northeast Atlantic Ocean during the past 130,000 years. Quat. Res. 29, 142–152.

Huang, S.P., Pollack, H.N., Shen, P.Y., 2008. A late Quaternary climate reconstruction based on borehole heat flux data, borehole temperature data, and the instrumental record. Geophys. Res. Lett. 35, L13703.

Lüthi, D., Le Floch, M., Bereiter, B., Blunier, T., Barnola, J.M., Siegenthaler, U., Raynaud, D., Jouzel, J., Fischer, H., Kawamura, K., Stocker, T.F., 2008. High-resolution carbon dioxide concentration record 650,000-800,000 years before present. Nature 453, 379–382.

Lambeck, K., Rouby, H., Purcell, A., Sun, Y., Sambridge, M., 2014. sea level and global ice volumes from the last glacial maximum to the Holocene. Proc. Natl. Acad. Sci. U.S.A. 111, 15296–15303.

Laskar, J., Robutel, P., Joutel, F., Gastineau, M., Correia, A.C.M., Levrard, B., 2004. A long-term numerical solution for the insolation quantities of the Earth. Astron. Astrophys. 428, 261–285.

Lea, D.W., Pak, D.K., Peterson, L.C., Hughen, K.A., 2003. Synchroneity of tropical and high-latitude Atlantic temperatures over the last glacial termination. Science 301, 1361–1364.

Lemieux-Dudon, B., Blayo, E., Petit, J.R., Waelbroeck, C., Svensson, A., Ritz, C., Barnola, J.M., Narcisi, B.M., Parrenin, F., 2010. Consistent dating for Antarctic and Greenland ice cores. Quat. Sci. Rev. 29, 8–20.

Liu, Z., Huang, S., Jin, Z., 2018. A last deglacial climate dataset comprising ice core data, marine data, and stalagmite data. Data in Brief, Submitted.

Liu, Z., Otto-Bliesner, B., He, F., Brady, E., Tomas, R., Clark, P., Carlson, A., Lynch-Stieglitz, J., Curry, W., Brook, E., 2009. Transient simulation of last deglaciation with a new mechanism for Bølling-Allerød warming. Science 325, 310–314.

Marcott, S.A., Bauska, T.K., Buizert, C., Steig, E.J., Rosen, J.L., Cuffey, K.M., Fudge, T.J., Severinghaus, J.P., Ahn, J., Kalk, M.L., McConnell, J.R., Sowers, T., Taylor, K.C., White, J.W., Brook, E.J., 2014. Centennial-scale changes in the global carbon cycle during the last deglaciation. Nature 514, 616–619.

Marcott, S.A., Clark, P.U., Padman, L., Klinkhammer, G.P., Springer, S.R., Liu, Z., Otto-Bliesner, B.L., Carlson, A.E., Ungerer, A., Padman, J., 2011. Ice-shelf collapse from subsurface warming as a trigger for Heinrich events. Proc. Natl. Acad. Sci. U.S.A. 108, 13415–13419.

McManus, J.F., Francois, R., Gherardi, J.-M., Keigwin, L.D., Brown-Leger, S., 2004. Collapse and rapid resumption of Atlantic meridional circulation linked to deglacial climate changes. Nature 428, 834–837.

Milanković, M., 1941. Kanon der Erdbestrahlung und seine Anwendung auf das Eiszeitenproblem (Canon of insolation and the ice-age problem), Section of Mathematical and Natural Sciences. Royal Serbian Academy of Sciences Speciales 633 pp.

Monnin, E., Indermuhle, A., Dallenbach, A., Fluckiger, J., Stauffer, B., Stocker, T.F., Raynaud, D., Barnola, J.M., 2001. Atmospheric CO_2 concentrations over the last glacial termination. Science 291, 112–114.

Mudelsee, M., 2000. Ramp function regression: a tool for quantifying climate transitions. Comput. Geosci. 26, 293–307.

Mudelsee, M., 2001. The phase relations among atmospheric CO_2 content, temperature and global ice volume over the past 420 ka. Quat. Sci. Rev. 20, 583–589.

Mudelsee, M., 2009. Break function regression: a tool for quantifying trend changes in climate time series. Eur. Phys. J. Spec. Top. 174, 49–63.

Nakamura, A., Yokoyama, Y., Maemoku, H., Yagi, H., Okamura, M., Matsuoka, H., Miyake, N., Osada, T., Adhikari, D.P., Dangol, V., Ikehara, M., Miyairi, Y., Matsuzaki, H., 2016. Weak monsoon event at 4.2 ka recorded in sediment from Lake Rara, Himalayas. Quat. Int. 397, 349–359.

Neftel, A., Oeschger, H., Staffelbach, T., Stauffer, B., 1988. CO_2 record in the Byrd ice core 50,000-5,000 years BP. Nature 331, 609–611.

Parrenin, F., Barker, S., Blunier, T., Chappellaz, J., Jouzel, J., Landais, A., Masson-Delmotte, V., Schwander, J., Veres, D., 2012. On the gas-ice depth difference (Δdepth) along the EPICA Dome C ice core. Clim. Past 8, 1239–1255.

Parrenin, F., Masson-Delmotte, V., Köhler, P., Raynaud, D., Paillard, D., Schwander, J., Barbante, C., Landais, A., Wegner, A., Jouzel, J., 2013. Synchronous change of atmospheric CO_2 and Antarctic temperature during the last deglacial warming. Science 339, 1060–1063.

Peck, V.L., Hall, I.R., Zahn, R., Elderfield, H., 2008. Millennial-scale surface and subsurface paleothermometry from the northeast Atlantic, 55-8 ka BP. Paleoceanography 23, PA3221.

Pedro, J.B., Rasmussen, S.O., van Ommen, T.D., 2012. Tightened constraints on the timelag between Antarctic temperature and CO_2 during the last deglaciation. Clim. Past 8, 1213–1221.

Pedro, J.B., van Ommen, T.D., Rasmussen, S.O., Morgan, V.I., Chappellaz, J., Moy, A.D., Masson-Delmotte, V., Delmotte, M., 2011. The last deglaciation: timing the bipolar seesaw. Clim. Past 7, 671–683.

Peltier, W.R., Fairbanks, R.G., 2006. Global glacial ice volume and Last Glacial Maximum duration from an extended Barbados sea level record. Quat. Sci. Rev. 25, 3322–3337.

Petit, J.R., Jouzel, J., Raynaud, D., Barkov, N.I., Barnola, J.-M., Basile, I., Bender, M., Chappellaz, J., Davis, M., Delaygue, G., Delmotte, M., Kotlyakov, V.M., Legrand, M., Lipenkov, V.Y., Lorius, C., Pépin, L., Ritz, C., Saltzman, E., Stievenard, M., 1999. Climate and atmospheric history of the past 420,000 years from the Vostok ice core, Antarctica. Nature 399, 429–436.

Raymo, M.E., Oppo, D.W., Curry, W., 1997. The mid-Pleistocene climate transition: a deep sea carbon isotopic perspective. Paleoceanography 12, 546–559.

Reimer, P.J., Baillie, M.G.L., Bard, E., Bayliss, A., Beck, J.W., Bertrand, C.J.H., Blackwell, P.G., Buck, C.E., Burr, G.S., Cutler, K.B., Damon, P.E., Edwards, R.L., Fairbanks, R.G., Friedrich, M., Guilderson, T.P., Hogg, A.G., Hughen, K.A., Kromer, B., McCormac, G., Manning, S., Ramsey, C.B., Reimer, R.W., Remmele, S., Southon, J.R., Stuiver, M., Talamo, S., Taylor, F.W., van der Plicht, J., Weyhenmeyer, C.E., 2004. IntCal04 terrestrial radiocarbon age calibration, 0-26 cal kyr BP. Radiocarbon 46, 1029–1058.

Rosen, J.L., Brook, E.J., Severinghaus, J.P., Blunier, T., Mitchell, L.E., Lee, J.E., Edwards, J.S., Gkinis, V., 2014. An ice core record of near-synchronous global climate changes at the Bølling transition. Nat. Geosci. 7, 459–463.

Schmittner, A., Galbraith, E.D., 2008. Glacial greenhouse-gas fluctuations controlled by ocean circulation changes. Nature 456, 373–376.

Shakun, J.D., Clark, P.U., He, F., Marcott, S.A., Mix, A.C., Liu, Z., Otto-Bliesner, B., Schmittner, A., Bard, E., 2012. Global warming preceded by increasing carbon dioxide concentrations during the last deglaciation. Nature 484, 49–54.

Siegenthaler, U., Stocker, T.F., Monnin, E., Lüthi, D., Schwander, J., Stauffer, B., Raynaud, D., Barnola, J.-M., Fischer, H., Masson-Delmotte, V., Jouzel, J., 2005. Stable carbon cycle-climate relationship during the Late Pleistocene. Science 310, 1313–1317.

Sigman, D.M., Hain, M.P., Haug, G.H., 2010. The polar ocean and glacial cycles in atmospheric CO_2 concentration. Nature 466, 47–55.

Skinner, L.C., Fallon, S., Waelbroeck, C., Michel, E., Barker, S., 2010. Ventilation of the deep Southern Ocean and deglacial CO_2 rise. Science 328, 1147–1151.

Stenni, B., Masson-Delmotte, V., Johnsen, S., Jouzel, J., Longinelli, A., Monnin, E., Röthlisberger, R., Selmo, E., 2001. An oceanic cold reversal during the last deglaciation. Science 293, 2074–2077.

Stern, J.V., Lisiecki, L.E., 2013. North Atlantic circulation and reservoir age changes over the past 41,000 years. Geophys. Res. Lett. 40, 3693–3697.

Stocker, T.F., Johnsen, S.J., 2003. A minimum thermodynamic model for the bipolar seesaw. Paleoceanography 18, 1087.

Svensson, A., Andersen, K.K., Bigler, M., Clausen, H.B., Dahl-Jensen, D., Davies, S.M., Johnsen, S.J., Muscheler, R., Parrenin, F., Rasmussen, S.O., Röthlisberger, R., Seierstad, I., Steffensen, J.P., Vinther, B.M., 2008. A 60000 year Greenland stratigraphic ice core chronology. Clim. Past 4, 47–57.

Veres, D., Bazin, L., Landais, A., Kele, H.T.M., Lemieux-Dudon, B., Parrenin, F., Martinerie, P., Blayo, E., Blunier, T., Capron, E., Chappellaz, J., Rasmussen, S.O., Severi, M., Svensson, A., Vinther, B., Wolff, E.W., 2013. The Antarctic ice core chronology (AICC2012): an optimized multi-parameter and multi-site dating approach for the last 120 thousand years. Clim. Past 9, 1733–1748.

Wang, J., Zhu, L., Wang, Y., Peng, P., Ma, Q., Haberzettl, T., Kasper, T., Matsunaka, T., Nakamura, T., 2017. Variability of the ^{14}C reservoir effects in Lake Tangra Yumco, Central Tibet (China), determined from recent sedimentation rates and dating of plant fossils. Quat. Int. 430, 3–11.

Wang, X., Auler, A.S., Edwards, R., Cheng, H., Ito, E., Wang, Y., Kong, X., Solheid, M., 2007. Millennial-scale precipitation changes in southern Brazil over the past 90,000 years. Geophys. Res. Lett. 34, L23701.

Wang, X., Auler, A.S., Edwards, R.L., Cheng, H., Cristalli, P.S., Smart, P.L., Richards, D.A., Shen, C.C., 2004. Wet periods in northeastern Brazil over the past 210 kyr linked to distant climate anomalies. Nature 432, 740–743.

Wang, Y.J., Cheng, H., Edwards, R.L., An, Z.S., Wu, J.Y., Shen, C.C., Dorale, J.A., 2001. A high-resolution absolute-dated late Pleistocene Monsoon record from Hulu Cave, China. Science 294, 2345–2348.

Wolff, E.W., 2012. Climate change: a tale of two hemispheres. Nature 484, 41–42.